Materials Today Bio 23 (2023) 100873

Contents lists available at ScienceDirect

Materials Today Bio

journal homepage: www.journals.elsevier.com/materials-today-bio

Emulsifying Lipiodol with pH-sensitive DOX@HmA nanoparticles for hepatocellular carcinoma TACE treatment eliminate metastasis

Qing Shi [a,1], Xingxing Zhang [a,b,1], Minmin Wu [a,1], Yuhan Xia [a], Yating Pan [a], Jialu Weng [a], Na Li [a,c,***], Xingjie Zan [a,c,*], Jinglin Xia [a,d,e,**]

[a] Key Laboratory of Diagnosis and Treatment of Severe Hepato-Pancreatic Diseases of Zhejiang Province, The First Affiliated Hospital of Wenzhou Medical University, Wenzhou, 325000, Zhejiang, China
[b] Shanghai University of Medicine & Health Sciences Affiliated Sixth People ' s Hospital South Compus, Shanghai, 201499, China
[c] Wenzhou Institute, Wenzhou Key Laboratory of Perioperative Medicine, University of Chinese Academy of Sciences, Wenzhou, 325001, China
[d] Liver Cancer Institute, Zhongshan Hospital of Fudan University, Shanghai, 200032, China
[e] National Clinical Research Center for Interventional Medicine, Shanghai, 200032, China

ARTICLE INFO

Keywords:
pH-sensitive nanoparticles
Hexahistidine-metal
Doxorubicin
Transcatheter arterial chemoembolization
Liver cancer

ABSTRACT

Lipiodol-based transcatheter arterial chemoembolization (TACE) is currently the predominant and first-line treatment option recommended by the global standard for unresectable hepatocellular carcinoma (HCC). However, the unstable emulsion of Lipiodol causes a substantial proportion of chemotherapy drugs to enter the circulation system, leading to poor accumulation in cancer tissues and unexpected side effects of chemotherapy drugs. Herein, we emulsified Lipiodol with a pH-sensitive drug delivery system assembled from hexahistidine and zinc ions (HmA) with a super-high loading capacity of doxorubicin (DOX) and a promising ability to penetrate bio-barriers for the effective treatment of HCC by TACE. *In vitro* tests showed that DOX@HmA was comparable to free DOX in killing HCC cells. Impressively, during the in vivo TACE treatment, the anti-tumor efficacy of DOX@HmA was significantly greater than that of free DOX, indicating that DOX@HmA increased the accumulation of DOX in tumor. Emulsifying Lipiodol with pH-sensitive DOX@HmA significantly inhibited cell regeneration and tumor angiogenesis and decreased the systemic side effects of chemotherapy, especially by suppressing pulmonary metastasis in liver VX2 tumors in rabbits by inhibiting epithelial–mesenchymal transition (EMT). Emulsifying tumor microenvironment-responsive drug delivery systems (DDSs) with Lipiodol could be a new strategy for clinical TACE chemotherapy with potentially enhanced HCC treatment.

1. Introduction

Hepatocellular carcinoma (HCC) is the sixth most commonly diagnosed cancer and the third most common cause of cancer-related mortality worldwide [1]. Lipiodol-based transcatheter arterial chemoembolization (TACE) is currently the predominant and first-line option recommended by the global standard for unresectable HCC because it is economical and patient-friendly. Typically, chemotherapy drugs are administered together with embolic agents into the tumor artery through a catheter [2–5]. The expected combined therapeutic effects simultaneously come from the chemotherapy drugs' killing ability and the embolic agents' ability to cut off blood supply to the tumor's blood vessels. Nonetheless, the microenvironment, ischemia, and hypoxia around the tumor tissue after TACE can induce a significant increase in angiogenic cytokines (such as vascular endothelial factor), resulting in high vessel leakage and the opening of the tumor's vascular collateral circulation [6]. In this case, the unstable emulsion of Lipiodol causes a substantial proportion of chemotherapy drugs to enter the

* Corresponding author. Key Laboratory of Diagnosis and Treatment of Severe Hepato-Pancreatic Diseases of Zhejiang Province, The First Affiliated Hospital of Wenzhou Medical University, Wenzhou, 325000, Zhejiang, China.
** Corresponding author. Key Laboratory of Diagnosis and Treatment of Severe Hepato-Pancreatic Diseases of Zhejiang Province, The First Affiliated Hospital of Wenzhou Medical University, Wenzhou, 325000, Zhejiang, China.
*** Corresponding author. Key Laboratory of Diagnosis and Treatment of Severe Hepato-Pancreatic Diseases of Zhejiang Province, The First Affiliated Hospital of Wenzhou Medical University, Wenzhou, 325000, Zhejiang, China.
E-mail addresses: minminwu@wzhospital.cn (M. Wu), lina0701@ucas.ac.cn (N. Li), zanxj@ucas.ac.cn (X. Zan), xiajinglin@fudan.edu.cn (J. Xia).
[1] **Note:** They contributed equally to this work.

https://doi.org/10.1016/j.mtbio.2023.100873
Received 27 September 2023; Received in revised form 5 November 2023; Accepted 17 November 2023
Available online 29 November 2023

circulation system, thus leading to poor accumulation in cancer tissues and unexpected side effects of chemotherapy drugs [7]. Even worse, the high expression level of angiogenic cytokines contributes to the great possibility of cancer metastasis, spreading HCC from the liver to other sites such as the lungs and brain, which accounts for most HCC-related deaths. Reportedly, only 15–55 % of patients are responsive to TACE treatment, with the median survival increasing from 16 to 20 months [8]. Therefore, the development of new strategies to improve therapeutic outcomes and reduce adverse effects remains challenging.

Inefficient delivery of anticancer drugs into the target tumor tissue results in poor TACE treatment outcomes, and various methods based on different techniques have been developed to improve therapeutic outcomes [9]. Using the sonoporation effect of sonication waves, Kim et al. [10]. reported that a Lipiodol-complexed microbubble conjugated with doxorubicin (DOX)-loaded nanoparticles penetrated deeply into the tumor through a leaky blood vessel near the microbubble and across the cell membrane through temporarily induced pores. Utilizing the ability of drug delivery systems (DDSs) to transform drug pharmacokinetics and the biodistribution of small molecular drugs [11–13], Liu et al. [14] synthesized periodic mesoporous organosilica-coated magnetite nanoparticles with excellent DOX-loading capacity to combine with Lipiodol to improve TACE treatment of unresectable liver cancer. Although these studies represent substantial advances in the field, they are often hampered by complex chemical syntheses and elaborate vector designs, making future clinical translation difficult.

The tumor microenvironment caused by metabolic changes in tumor cells is acidic, resulting from anaerobic glycolysis being the primary means of energy release in tumor cells rather than oxidative phosphorylation and a significant increase in lactic acid load in the extracellular environment [15,16]. Recently, pH-sensitive DDSs have received considerable attention owing to their ability to target the delivery of anticancer drugs to tumor sites [17,18]. However, very few studies have demonstrated the combination of pH-sensitive DDSs with Lipiodol for TACE treatment [19]. In our lab, we previously developed smart nanodrugs generated by the poly-his6-boligostyrene and zinc coordination self-assembly (HmA) strategy, which have the advantages of tumor-specific delivery, higher loading capacity, and pH-sensitive release for tumor-targeting [20,21]. In addition, HmA exhibits a promising ability to penetrate various biobarriers, such as cellular membranes and the corneal barrier, for delivering small molecular and protein drugs [22–27]. Herein, we present HmA loaded with DOX (DOX@HmA) to enhance the effects of TACE against liver cancer. HmA has excellent biocompatibility and stability, a high loading capacity, and DOX phagocytic ability. It also sustains and delays pH-sensitive drug release behavior in an acidic pH environment. The combination of HmA and DOX killed hepatocellular carcinoma cells *in vitro*. Our data demonstrated that emulsifying Lipiodol with DOX@HmA presented significant anti-tumor efficacy in *in vivo* TACE treatment, showing decreased systemic side effects of chemotherapy and pulmonary metastasis in liver VX2 tumors of rabbits by inhibiting epithelial-mesenchymal transition (EMT) formation.

2. Materials and methods

2.1. Materials

The VX2 tumor cell line was purchased from Jennio Biotech (China). HepG2 and Huh7 cell lines, LO2 cell lines, and special culture media were obtained from iCell (China). Dulbecco's modified Eagle's medium (DMEM), fetal bovine serum (FBS), penicillin-streptomycin (Pen-Strep), and trypsin-EDTA solution were supplied by Gibco (USA). Hexahistidine (His_6) was synthesized by Zhuantai Biocom (China). All chemicals, including 4-(2-hydroxyethyl)-1-piperazineethanesulfonic acid (HEPES), polyvinylpyrrolidone (PVPON, Mw~58k), zinc nitrate hexahydrate, sodium hydroxide, and hydrochloric acid, were provided by Aladdin (China). Cell counting kit-8 (CCK-8) was purchased from GLPBIO (USA). Live/dead cell staining kits were obtained from APExBIO (USA). The Annexin V-Fluorescein Apoptosis Assay Kit was supplied by Multisciences (Beijing, China). DOX, crystal violet ammonium oxalate, methyl thiazolyl tetrazolium (MTT), and phosphate-buffered saline (PBS) were purchased from Solarbio (China). Actin-Tracker Green-488, Hoechst 33342, and colorimetric TUNEL Apoptosis Assay Kits were provided by Beyotime (China). Lipiodol was obtained from Guerbet (France). Ki-67 antibodies and vascular endothelial growth factor (VEGF) were obtained from Abcam (Cambridge, UK).

2.2. Synthesis and characterization of DOX@HmA NPs

DOX was packed into HmA NPs via the following procedure: Briefly, Zn $(NO_3)_2$ (94 μL, 0.1 M) was added to 1 mL of HEPES buffer solution (pH 8.0) containing 4 mg of DOX, 3.9 mg of His_6, and 5.0 mg of PVP. The packaging procedure was ultrasonicated at 4 °C for 10 min, and the NPs were collected by centrifugation (14000 rpm, 15 min). Finally, the pellet was washed three times with deionized water, redispersed by ultrasonication, and stored in 1 mL of water at 4 °C before testing (stock solution).

Diluting 100 μL of stock solution into 1 mL of water, the particle size, dispersity coefficient PDI, and surface zeta potential of the NPs (HmA and HmA@DOX) were examined using a Zeta-sizer Nano ZS instrument (Malvern, UK). For the scanning electron microscopy (FE-SEM, Hitachi, SU8010) test, the 5 μL NPs were dropped onto a silicon wafer, fully dried, then gold sprayed. The 2-μL, 100-times diluted stock solution was dropped onto the copper grid coated with carbon film and observed by field emission transmission electron microscopy (TEM, Talos F200S FEI) after it had completely dried. After the DOX and NPs were diluted, the absorbance of the samples was measured using an ultraviolet spectrophotometer.

2.3. Encapsulation efficiency of DOX@ HmA

According to a previous report, with an excitation wavelength of 479 nm, an emission wavelength of 587 nm was used for quantitative analysis using a Thermo Scientific Microplate Reader. The encapsulation efficiency (EE%) and loading capacity (LCwt%) of DOX were directly determined three times according to a previously reported method by the following equations:

$$EE\% = \frac{Vol_o * A_o - Vol_s * A_s}{Vol_o * A_o} * 100\%$$

$$LCwt\% = \frac{W_{DOX} * EE\%}{W_{DOX@HmA} * Yield(\%)} * 100\%$$

where Vol_O and Vol_S represent the volumes of the original and supernatant solutions, respectively, and A_O and A_S represent the absorbances of DOX at the corresponding positions in the original and supernatant solutions, respectively. $W_{added\ drug}$ and $W_{DOX@HmA}$ are the weights of DOX and DOX@polyhistidine, respectively.

2.4. In vitro release

DOX release from DOX@HmA NPs was performed in PBS at different pH values according to a previously described method [28]. Briefly, 1 mL of DOX@HmA NPs (containing 2 mg of DOX) were placed in a dialysis tube with a cut-off molecular weight of 1 kDa. Then, in a constant-temperature shaker at 400 rpm and 37 °C, the dialysis tubes were incubated in 19 mL of PBS solution (pH = 7.4, 6.5, and 4.5). The test solution (0.5 mL) was removed at the desired time point and a fresh buffer solution (0.5 mL) with the same pH was added. The cumulative release was calculated using the following equation:

$$\frac{C_{t,DOX} * V_t + \Sigma_i C_{i,DOX} * V_i}{W_{total,DOX}} * 100\% = \frac{C_{t,DOX} * V_t + \Sigma_i C_{i,DOX} * V_i}{m_{o,DOX} * EE_{DOX}(\%)} * 100\%$$

where C_t and C_i represent the concentration of DOX at the test time point (t) and before the (t) time point (i) in the mother liquor, respectively. V_t and V_i represent the volumes of the mother liquor and waste mother liquor at (t) time t (0.5 ml), respectively, and $W_{total,DOX}$ are the original values of DOX for the HmA particles.

2.5. Biocompatibility

HepG2 cells, Huh7 cells, LO2 cells were seeded in 96-well plates at a density of $1*10^4$ cells/well in DMEM (containing 10 % FBS) and Huh7 special culture medium in 5 % CO_2 at 37 °C. After culturing for 12 h, removing the culture medium, and washing with PBS, we added different concentrations (0 μg/ml, 25 μg/ml, 50 μg/ml, 100 μg/ml, 150 μg/ml) of HmA NPs suspension with 10 % DMEM for 24 h. Cell biocompatibility was evaluated using the CCK-8 assay and a live staining kit, according to the manufacturer's protocol.

2.6. Cell uptake efficiency

HepG2 and Huh7 cells were seeded in confocal dishes at a density of 2×10^5 cells/wells. After 12 h of incubation, DOX and DOX@HmA (DOX concentration of 1 μg/ml), including DMEM, were added and incubated with HepG2 cells and Huh7 cells for another 3 h. The cytoskeletal structures of the cells were stained with Actin-Tracker Green and DAPI for confocal laser scanning microscopy (A1 Nikon, Japan).

2.7. Cell toxicity

HepG2 and Huh7 cells were seeded into 96-well plates at a density of 10 000 cells/well. After 12 h, different concentrations (0 μg/ml, 6.25 μg/ml, 12.5 μg/ml, 25 μg/ml, 50 μg/ml, and 100 μg/ml) of DOX@HmA NPs suspension with DMEM (10 % FBS) were added and cultured with cells for another 24 h. The MTT assay was performed according to the manufacturer's protocol. HepG2 and Huh7 cells were seeded into 6-well plates. DOX and DOX@HmA NPs were then added to the cell culture supernatant. After being cocultured for 24 h, live staining and the Annexin V-Fluorescein Apoptosis Assay Kit were performed and imaged according to the manufacturer's instructions. After coculturing for 14 d, the cells were fixed with paraformaldehyde, stained with 1 % crystal violet overnight, washed three times with PBS, and photographed for observation.

2.8. Animals

2.8.1. Animals models

All animal experiments were conducted in accordance with the guidelines approved by the Ethics Committee of the Wenzhou Institute, University of Chinese Academy of Sciences (WIUCAS22091901). All the rabbits were housed individually in steel cages at the Wenzhou Institute, University of Chinese Academy of Sciences Laboratory Animal Center, under standard feeding conditions throughout the experimental period. Nine New Zealand white rabbits with body weights of 2.0–2.5 kg were purchased from the Wenzhou Institute, University of Chinese Academy of Sciences Laboratory Animal Center. All rabbits were randomly distributed into three groups according to the experimental design. Each animal was implanted with a single tumor in the left lobe of the liver, based on previous reports [29–31]. Briefly, rabbits were anesthetized with 3 % pentobarbital sodium (0.5 ml/kg). When anesthesia was administered, all rabbits underwent minimally invasive laparotomies after shaving and disinfecting the area below the xiphoid. Under sterile conditions, VX2 rabbit tumor tissue without central necrosis was implanted into the left lobe of the liver to establish pre-invasive tumors. Subsequently, the abdominal wall was sutured, and 200, 000 units of streptomycin were injected intramuscularly to prevent infection. VX2 tumors developed *in vivo* for 10–14 d prior to treatment.

2.8.2. In vivo CT

All rabbits were subjected to contrast-enhanced CT scans on day 0 (baseline before treatment) and day 14 following TACE in all groups. A clinical CT scanner (Siemens Healthcare, SOMATON go. Top, Germany) was used for preoperative and postoperative diagnosis and evaluation. After anesthetization, the animals were placed on their backs for CT imaging. The parameters of the CT scan were acquired (arterial phase: 15s; venous phase: 30s; delayed phase: 60s; injection speed of iodixanol: 0.3 ml/s, total dose of iodixanol: 7 ml, section thickness: 2.5 mm, voltage: 120 kV). The images were assessed using a professional picture archiving and communication system (PACS) workstation (M-view; Marotech, Seoul, Korea).

2.8.3. TACE procedures

After the diagnosis of liver tumors by CT imaging, all rabbits were randomly distributed into three groups and treated with TACE surgery according to different treatments: N**S group, Lipiodol + DOX group**, and **Lipiodol + DOX@HmA NPs group**. TACE was performed under fluoroscopic guidance using a previously reported method [32]. Briefly, the rabbits were anesthetized with 3 % pentobarbital sodium (0.5 ml/kg). The rabbits were fixed to the operating table in the supine position, shaved, and disinfected. A surgical incision of approximately 6–8 cm was made in the most visible area of femoral artery pulsation, and the femoral artery was isolated by approximately 3–4 cm. The femoral artery was punctured using a puncture needle with a 4-F catheter sheath (Cook Company, USA), which was pulled out, and the catheter sheath was fixed on both sides of the femoral artery. Next, a microguidewire and microcatheter (Progreat, Terumo, Japan) were slowly introduced into the catheter sheath. When the microcatheter was inserted into the abdominal aorta, iodixanol was injected for digital subtraction angiography (DSA; Siemens, Germany) to observe the distribution of the abdominal vessels and the arteries supplying the liver tumor. To identify the artery supplying the liver tumor, a microguidewire and microcatheter were slowly introduced into the target vessel for further treatment. According to the DOX concentration, DOX@HmA NPs (actual DOX dose: 2 mg/kg) and DOX (2 mg/kg) were dissolved in NS and mixed with Lipiodol for injection. The animals in different groups were then injected with the corresponding treatments using a microcatheter. Next, the microguidewire and microcatheter were slowly pulled out, the two ends of the femoral artery were ligated, and the surgical wound was sutured layer by layer.

2.8.4. Pathological evaluation

After CT scanning, the heart, liver, spleen, lung, kidney, tumor and paracancerous tissues were extracted, then deparaffinized, hydrated, and cut into a 5 μm-thick sections. To detect and assess tumor necrosis and proliferation, H&E, tunnel staining, immunofluorescent (IF) staining with Ki-67 (1:200) antibodies, and VEGF (1:200) antibodies were performed, respectively.

2.8.5. Liver, renal and heart function

Blood samples were collected from all rabbits to evaluate DOX toxicity. Aspartate aminotransferase (AST), alanine aminotransferase (ALT), blood urea nitrogen (BUN), creatinine (CR), creatine kinase (CK), and creatine kinase-MB (CK-MB) levels were measured to assess liver, renal, and heart function according to the manufacturer's instructions. White blood cells (WBC) and platelets (PLT) were measured to evaluate myelosuppression using an automated hematology analyzer (BC-5000 Vet).

2.9. Statistical analysis

Experimental data were expressed as the mean ± SD, and accessed by using GraphPad Prism 9.0 (GraphPad, USA). Statistically significant differences between the two groups were analyzed using ANOVA. Statistical significance was determined by $^*P < 0.05$, and $^{**}P < 0.01$

(Origin Lab Software, USA).

3. Results and discussion

3.1. Synthesis and characteristics of DOX@HmA

The HmA and DOX@HmA NPs prepared by mixing hexahistidine (His6) with Zn^{2+} and DOX via ultrasonication at pH 8 were observed by SEM (Fig. 1a) and TEM (Fig. 1b). The results indicated that the addition of DOX did not change the morphology of the NPs, which exhibited an irregular shape. The average particle sizes of HmA and DOX@HmA NPs were 91.4 nm and 135.5 nm, respectively, showing a narrow size distribution (lower than 0.25 in Fig. 1d) and a positive charge (16.3 mV and 19.1 mV in Fig. 1e). These data suggested that the loading of DOX into HmA did not significantly increase the size of NPs, with a slight increase in size distribution and zeta potential, which was similar to former research [28].

Compared with the original absorbance peak of DOX at 482 nm (brown line in Fig. 1g), the absorbance of the DOX@HmA supernatant was significantly lower, and the absorbance of DOX@HmA was slightly lower (Fig. 1g), suggesting that DOX was successfully loaded into HmA. Two main parameters, encapsulation efficiency (EE) and loading capacity (LC), were assessed to evaluate the HmA carrying profile. Both the EE and LC increased with increasing DOX concentration, reaching as high as 67 % EE and 41 % LC at 4 mg/mL DOX (Fig. 1h). Compared with other reports, through multiple interaction forces and coordination functions, HmA NPs have higher small-molecule drug loading.

The in vitro drug release behavior of the prepared DOX@HmA was evaluated under different pH conditions (pH 4.5, 6.5, and 7.4) using PBS as the release medium. As shown in Fig. 1j, the release rate in the first 24 h was greater than 40 % at pH 4.5 and pH 6.5, but only 28.6 % at pH 7.4. On day 14 of the experiment, DOX was released at pH 7.4, with a release rate of 53.4 %, 74 % at pH 6.5, and 83.9 % at pH 4.5. In a slightly acidic tumor microenvironment, the release of DOX was faster, indicating that DOX responds to pH via continuous release from DOX@HmA NPs. The slow, continuous, and pH-sensitive release of DOX can maintain an effective drug concentration in the tumor and produce sustained antitumor effects.

3.2. Biocompatibility assessment

To evaluate the cytotoxicity of HmA in vitro, HmA with different concentrations (0, 25, 50, 100, 150 μg/mL) were incubated with LO2, HepG2, and Huh7 cells for 24 h. There was no statistically significant difference in the relative cell viability at each concentration (Fig. 2a–c). Live-cell staining was performed to evaluate the cytotoxicity of HmA in

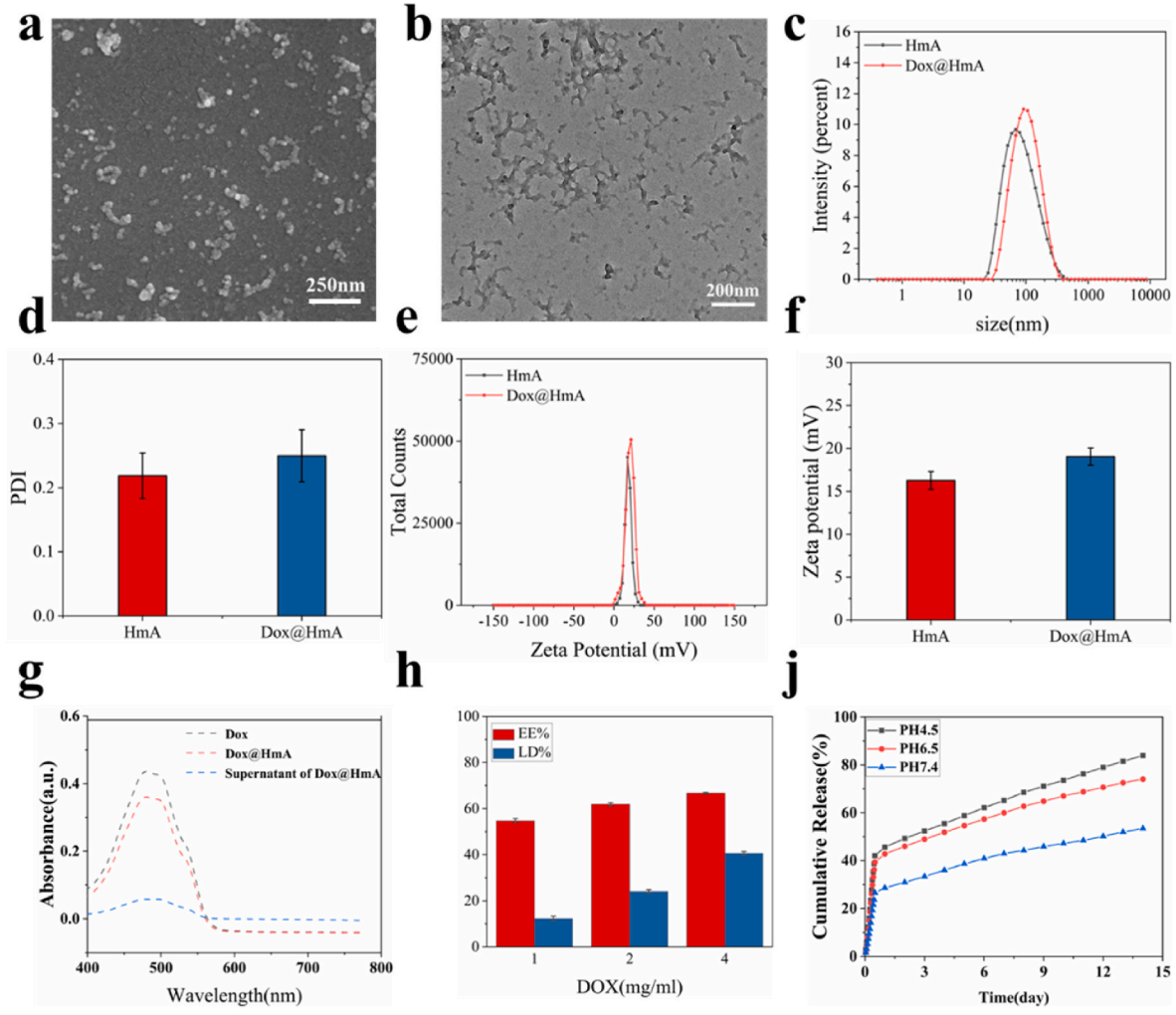

Fig. 1. Physicochemical properties of Dox-loaded nanoparticles. (a) The images of scanning electron microscopy (SEM) for Dox@HmA. (b) The images of transmission electron microscopy (TEM) for Dox@HmA. (c–f) Size distribution and Zeta potential of HmA and Dox@HmA particles. (g) UV–vis absorbance of Dox, Dox@HmA and supernatant of Dox@HmA. (h) EE% and LC% of Dox@HmA particles; (j) The in vitro release curve of doxorubicin in Dox@HmA by using different pH conditions (pH 4.5, 6.5, 7.4) of PBS at different times.

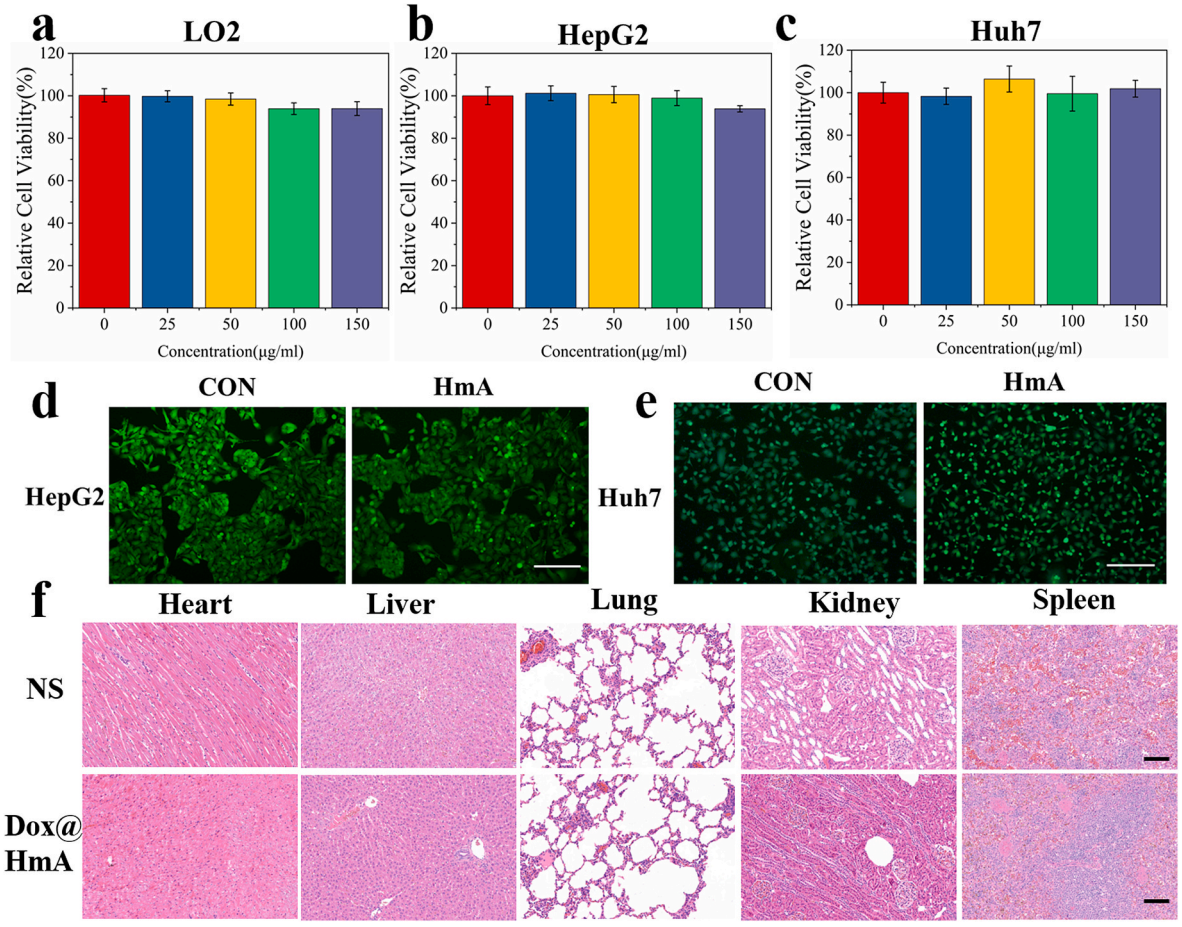

Fig. 2. The biocompatibility of HmA nanoparticles. (a–c) Cell viabilities of LO2 (a), HepG2 (b) and Huh7 (c) after treatment with different concentrations of Dox@HmA particles for 24 h. (d–e) The fluorescence of HepG2 (d) and Huh7 cells (e) intensities by Live cell staining were co-incubated with DMEM (10%FBS) and HmA for 24h. (f) The HE staining of heart, liver, lung, kidney, spleen in NS group and Dox@HmA group. All Scale bars are 100 μm.

HepG2 and Huh7 cells. The fluorescence intensity in the HmA group was similar to that in the control group (without HmA) (Fig. 2d and e). To further evaluate the biosafety of DOX@HmAs, H&E staining was performed on the heart, liver, lungs, spleen, and kidneys treated with DOX@HmAs for 14 d, which proved that DOX@HmAs had no influence on these organs (Fig. 2f). These results indicated that HmA is non-toxic and has excellent biocompatibility with cells and animals.

3.3. Cellular uptake

The cellular uptake of DOX released by DOX and DOX@HmA NPs in HepG2 and Huh7 cells was investigated using confocal laser scanning microscopy. There was no significant difference in the fluorescence intensities between the DOX and DOX@HmA groups (Fig. 3a and b). These results indicated that DOX encapsulated by HmA NPs exhibited stronger

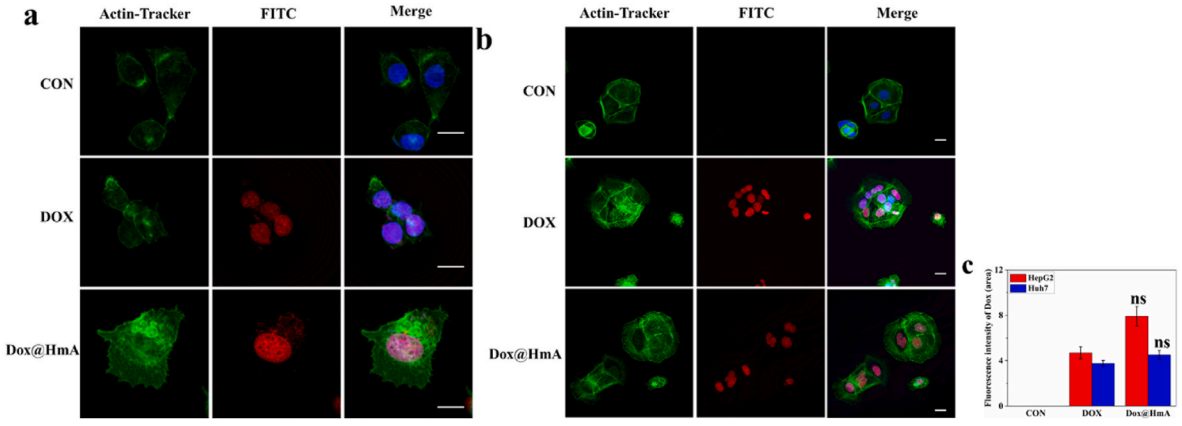

Fig. 3. The cellular uptake of DOX released by DOX and Dox@HmA to HepG2 and Huh7 cells by the confocal laser scanning microscopy. (a, b) The fluorescence staining images of HepG2 (a) and Huh7 (b) after co-incubation with DMEM, DOX, Dox@HmA for 3h; Cytoskeleton (green), Nucleus (blue), DOX (red). All scale bars are 20 μm. (c) Corresponding quantitative fluorescence intensity of DMEM, DOX and Dox@HmA in HepG2 and Huh7 cells (ns. represents no statistical difference vs DOX group). (For interpretation of the references to color in this figure legend, the reader is referred to the Web version of this article.)

endocytosis and that HmA NPs did not influence the phagocytic ability of DOX.

3.4. Cell viability assessment of DOX@HmA in vitro

Cytotoxicity is a key factor in the development of drug-loaded NPs. CCK-8, clone formation assay, live cell staining kit, and Annexin V/PI flow cytometry were used to evaluate the effect of DOX and DOX@HmA NPs on HepG2 and Huh7 cells. Compared with the control group (0 μg/ml), the cell viability of different concentrations of DOX and DOX@HmA all decreased after 24 h on two kinds of cells (Fig. 4a and b). The clone formation assay showed that the DOX and DOX@HmA groups had the lowest number of clonal colonies compared with the control after 14 d of co-incubation (Fig. 4c). In addition, the results of live cell staining were consistent with the results of the clone formation assay and MTT assay (Fig. 4d and e), but there was no significant difference between the DOX and DOX@HmA groups.

Annexin V/PI flow cytometry was performed to detect apoptosis in the HepG2 and Huh7 cells after treatment with DOX or DOX@HmA for 24 h. As shown in Fig. 4f and g, after 24 h of co-incubation with DOX and DOX@HmA NPs, the concentration of apoptotic HepG2 cells was 25.1 % and 28.8 %, and that of Huh7 cells was 20.2 % and 18.5 %, respectively. The results showed that the total number of apoptotic cells in the DOX@HmA NPs group was not significantly different from those in the DOX groups of HepG2 and Huh7 cells.

These results indicated that the combination of HmA and DOX could

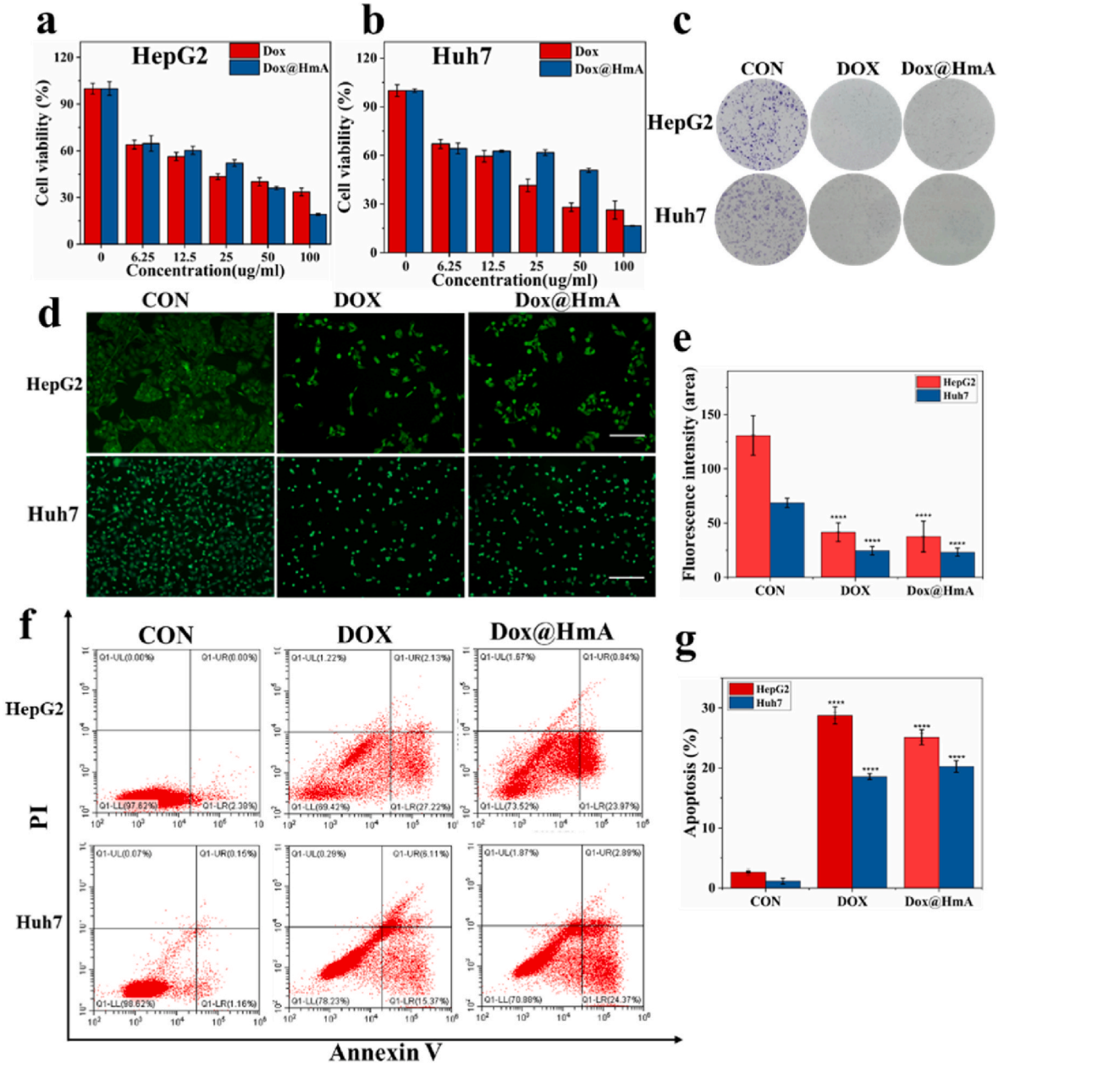

Fig. 4. Cytotoxicity and in vitro inhibitory effect of DOX and Dox@HmA. (a–b) The inhibitory effect of different concentration DOX and Dox@HmA to HepG2 and Huh7 cells was detected by MTT assay after co-incubation 24 h. (c) The images of clone formation assay after 14 d of co-incubation with HepG2 and Huh7 cells. (d–e) The microscopy of Liver cell staining and corresponding quantitative results of DMEM, DOX and Dox@HmA were co-incubated with HepG2 and Huh7 cells for 24 h. The scale bar was 100 μm. (f) The apoptosis of HepG2 and Huh7 cells after 24 h treatment by DMEM, DOX and Dox@HmA were detected via FITC-Annexin V/PI Flow Cytometry (upper and lower right quadrants represent late and early apoptotic cells), and the corresponding quantitative results (g), HepG2 and Huh7. (****P < 0.0001 vs CON group).

produce comparable anti-tumor efficacy in hepatocellular carcinoma.

3.5. TACE treatment

All tumor-bearing rabbits underwent contrast-enhanced CT 7 d after the in situ injection of VX2 tumor cell masses to confirm successful modeling, received TACE treatment, and were followed up for 2 weeks to assess the efficacy of the intervention treatment (Fig. 5a). As shown in Fig. 5b and c, the VX2 tumor masses were transplanted into the left lobe of the liver, the femoral artery of the rabbits was isolated, and a 4-F catheter sheath was placed in the femoral artery (Fig. 5c). Thereafter, VX2 tumor-bearing rabbits were injected with DOX@HmA NPs and Lipiodol through a microcatheter to implement the TACE treatment process under DSA guidance (Fig. 5d and e). More importantly, the NPs prepared in our study were targeted for delivery into the tumor supply artery, which was also selectively embolized by Lipiodol based on the DSA results (Fig. 5e).

3.6. The anti-tumor efficacy assessment in vivo

The therapeutic efficacy of DOX@HmA NPs and Lipiodol was evaluated according to variations in tumor volume via contrast-enhanced CT scans. Representative contrast-enhanced CT images of rabbits in each group before and 2 weeks after TACE are shown in Fig. 6a. In the NS group, the results showed that the average tumor volume was augmented 2 weeks post-treatment (Fig. 6a). Compared to the NS group, the results showed that traditional TACE treatment, namely the DOX and Lipiodol groups, also produced a certain anti-tumor effect (Fig. 6a). The DOX@HmA NPs and Lipiodol groups exhibited a significant inhibitory effect on tumor proliferation and Lipiodol deposition. The results indicated that, as a drug delivery system, HmA NPs increased the anti-tumor efficacy of DOX and augmented the deposition of Lipiodol in TACE

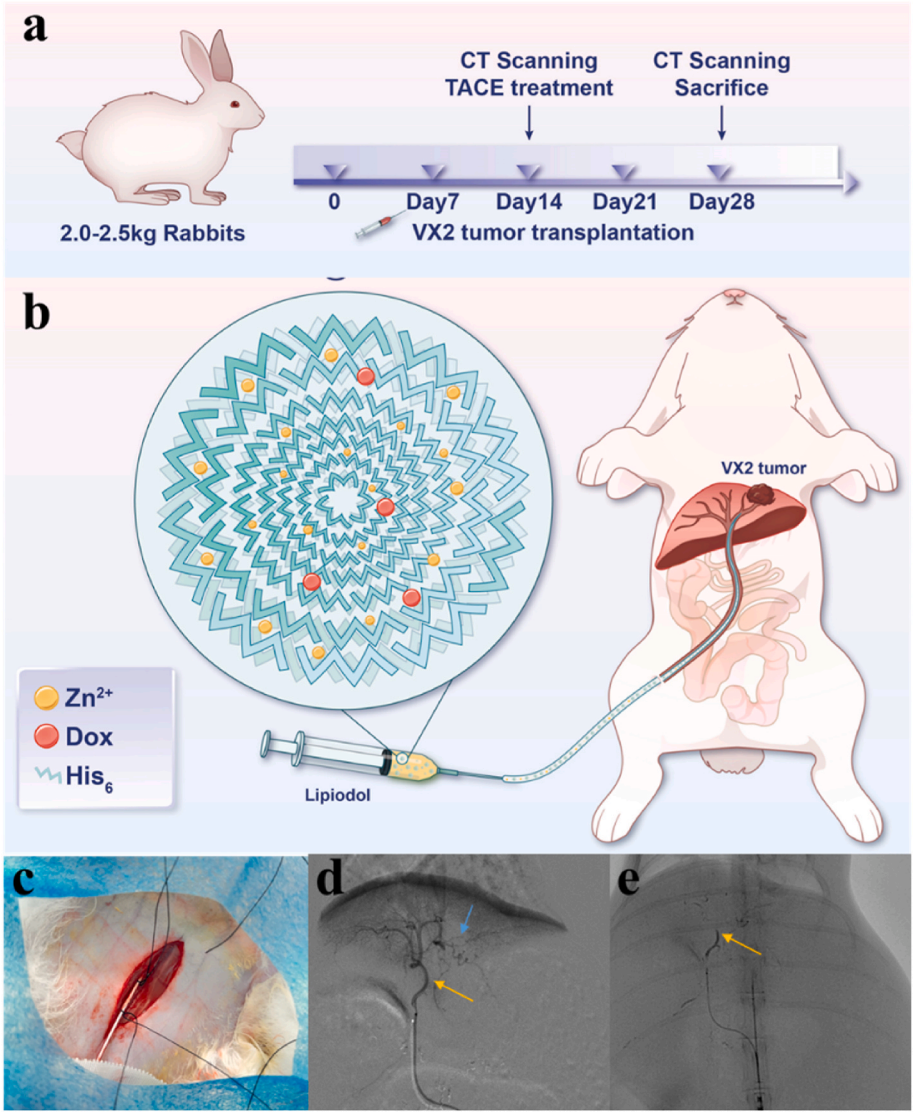

Fig. 5. Flow chart of in vivo research and TACE treatment process. (a) The tumor-bearing rabbits underwent CT scan one week after being transplanted VX2 tumor cells to confirm the successful modeling, then received TACE treatment, and followed up for 2 weeks to determine the efficacy of intervention. (b) Schematic diagram of the TACE treatment process, all the rabbits were undergoing laparotomy and expose their liver, VX2 tumor were transplanted into left lobe of liver, slowly introduced microcatheter into the target vessel, then injected Dox@HmA NPs and Lipiodol into the left hepatic artery to complete TACE treatment. (c) The femoral artery was isolated and punctured through a puncture needle with a 4-F catheter sheath. (d–e) All rabbits are treated, and confirmed whether the tumor supplying artery was embolized and infused with Lipiodol and nanoparticles under the guidance of DSA after the completion of TACE treatment. The yellow arrows represent left hepatic artery, and the blue arrow represents tumor vessel. (For interpretation of the references to color in this figure legend, the reader is referred to the Web version of this article.)

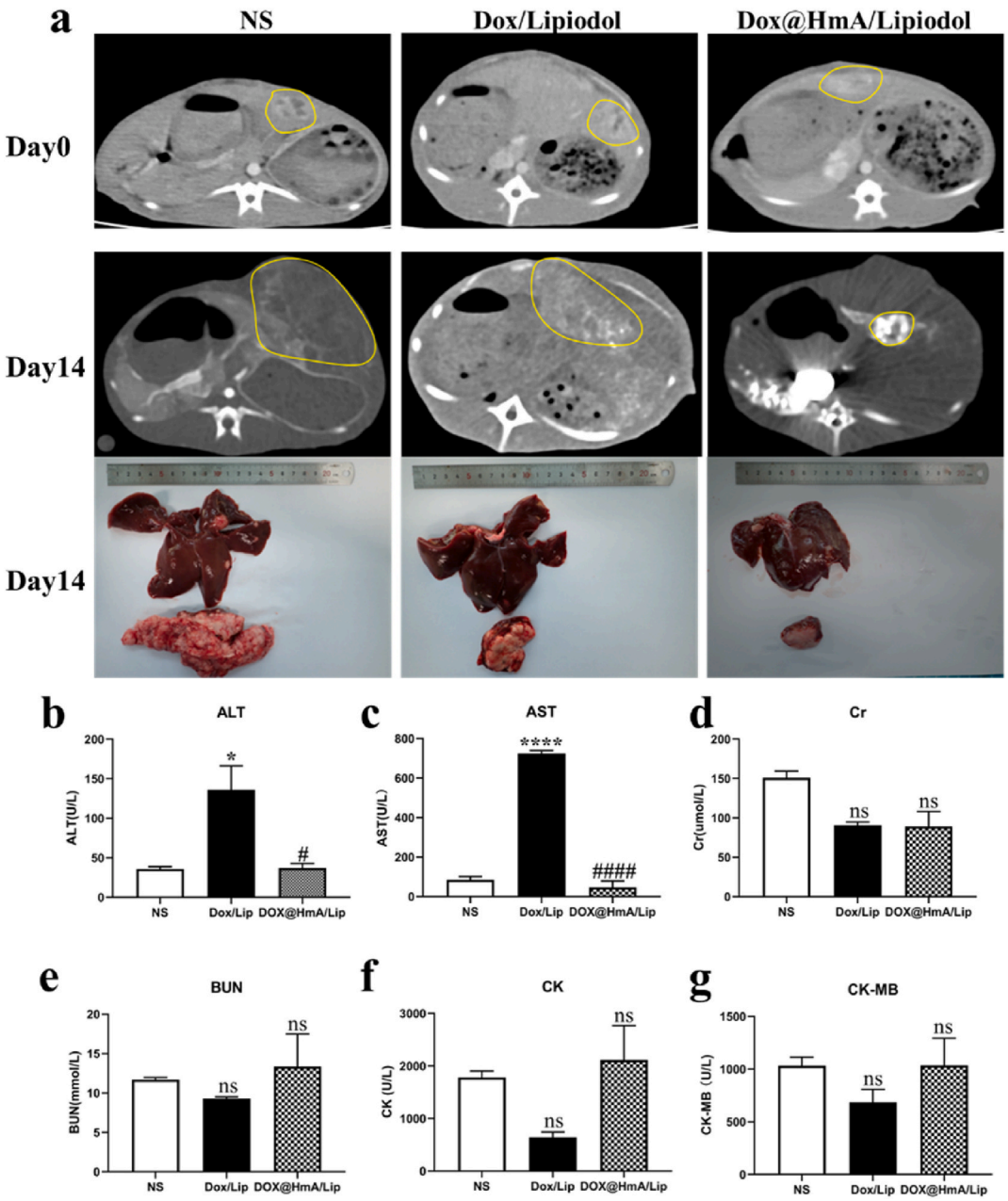

Fig. 6. Evaluation of the in vivo anti-tumor efficacy of NS, Dox/Lipiodol, Dox@HmA/Lipiodol based on CT scan follow-up. **(a)** Representative CT images of rabbits in each group before and 2 weeks after TACE treatment, which could be used to evaluate assess the therapeutic efficacy of NS, Dox/Lipiodol, Dox@HmA/Lipiodol group. Representative tumor images and macroscopic views of the VX-2 tumor of each group 2 weeks after TACE treatment. **(b–g) The ALT, AST, Cr, BUN, CK, CK-MB evaluation** of NS, Dox/Lipiodol, Dox@HmA/Lipiodol groups. (*P < 0.05, ****P < 0.0001 vs NS group; $^{\#}$P < 0.05, $^{\#\#\#\#}$P < 0.0001vs Dox/Lip group.).

treatment.

The most common side effects of chemotherapy are impaired liver, heart, and kidney functions. ALT and AST levels are commonly used to evaluate liver function. Compared to the DOX and Lipiodol groups, DOX@HmA NPs significantly decreased the liver damage induced by DOX (Fig. 6b and c). Cr, BUN, CK, and CK-MB levels are typically used to assess kidney and heart function. As shown in Fig. 6d–g, compared with the NS groups, TACE with DOX and **DOX@**HmA did not damage kidney and heart function. Therefore, the results showed that HmA NPs could significantly protect the liver from DOX-induced damage and had no effect on the kidney or heart.

3.7. Histopathology changes in tumors

All rabbits were sacrificed, and tumor tissues were collected for pathological staining 14 day after TACE treatment. As shown in Fig. 7a, the nuclei in the tumor regions of the NS group presented a tightly packed arrangement according to HE staining. In contrast, the **DOX@**HmA/Lipiodol group showed much larger necrotic areas than the DOX/Lipiodol group. Furthermore, Ki-67 is the main marker of the proliferative activity of tumor cells [33]. The relative fluorescence intensity of Ki-67-positive areas in the NS, DOX/Lipiodol, and **DOX@**HmA/Lipiodol groups were 105.44 ± 13.38, 52.176 ± 15.39, 22.39 ± 5.80, respectively. The relative fluorescence intensity of the Ki-67-positive area in the **DOX@**HmA/Lipiodol group was significantly lower than that in the other two groups, indicating that **DOX@**HmA has

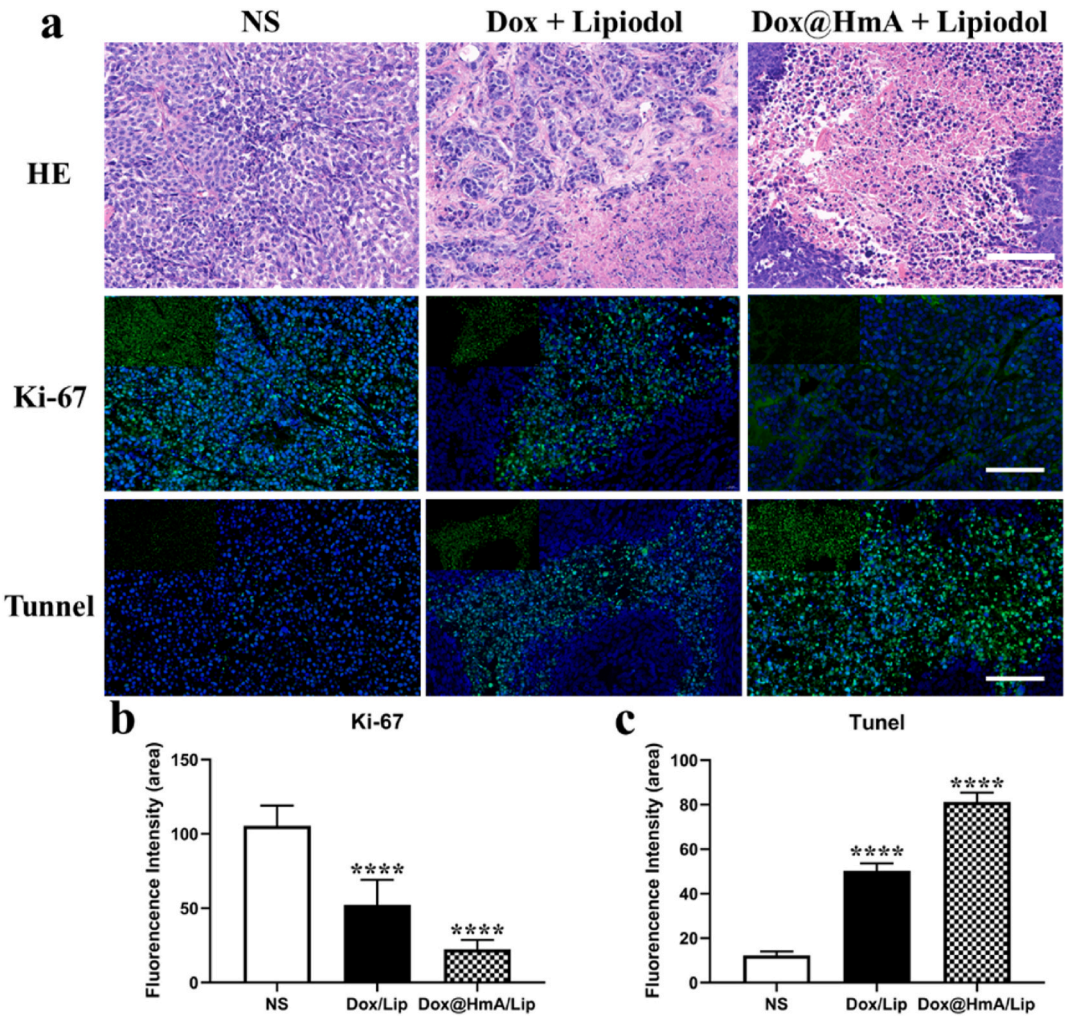

Fig. 7. Histological analysis of tumors in VX2 tumor-bearing rabbits 2-weeks after TACE treatment. **(a)** The representative images of the hematoxylin-eosin (HE) staining, Ki-67 and TUNEL immunofluorescence (IF) staining of tumor tissues for different groups. HE staining was used to observe the changes in the basic state of the tumors. **(b)** The index of Ki-67-positive area in each group was calculated. Data were presented as mean ± SD (n = 3). **(c)** The index of Tunnel-positive area in each group was calculated as a ratio of the apoptotic cell number to the total tumor cell number in each field of view. Data were presented as mean ± SD (n = 3). Scale bar represents 100 μm. (***P < 0.001, ****P < 0.0001).

better anti-tumor efficacy on tumor cell proliferation (Fig. 7b). The apoptotic activity of the tumor cells was tested using TUNEL staining. The relative fluorescence intensity of TUNEL-positive areas in the NS, DOX/Lipiodol, and **DOX@**HmA/Lipiodol groups were 12.33 ± 3.85, 50.28 ± 7.47, 81.21 ± 9.45, respectively. These results suggest that **DOX@**HmA/Lipiodol-treated rabbits achieved the highest apoptosis among all the groups (Fig. 7c). The results of Ki-67 and TUNEL IF staining were consistent, indicating that **DOX@**HmA/Lipiodol significantly promoted tumor apoptosis compared with DOX/Lipiodol, further suggesting that the assembly of HmA NPs and DOX could produce combined anti-tumor efficacy.

3.8. Lung metastasis

Metastasis, the ultimate and most lethal manifestation of cancer, refers to the growth of cancer cells in organs distant from their site of origin. The vast majority of cancer patients die from metastatic disease rather than from primary tumors [34]. Lung metastasis is the most common form of distant metastasis in liver cancer. Early detection may be attributed to tumor seeding during implantation, and can be identified in 16 % of lung cases two weeks after liver inoculation [35]. Therefore, we detected lung metastases from liver VX2 tumors by CT scanning. As shown in Fig. 8a, in the NS and DOX/Lipiodol groups, the representative CT images showed more metastatic lesions in the lungs. However, in the **DOX@**HmA/Lipiodol group, only a few metastatic lesions were observed in the lungs on the CT images. In addition, HE staining of lung tissues from different groups was performed to observe metastatic nodules in the lungs (Fig. 8b and c). In the NS and DOX/Lipiodol groups, there were numerous metastatic lesions in the lungs, but in the **DOX@**HmA/Lipiodol group, only a few metastatic lesions in the lungs were observed (Fig. 8b). As depicted in Fig. 8c, the DOX@HmA/Lipiodol group exhibited a significant reduction in lung metastases compared to the other two groups, demonstrating a statistically significant difference. In addition, DOX and **DOX@**HmA decreased the number of WBCs but not PLTs (Fig. 8d and e), which possibly resulted from tumor inhibition. Thus, the results of HE staining were consistent with the CT scanning images, showing that the DOX@HmA/Lipiodol group exhibited superior inhibition efficacy for lung metastasis compared with the DOX/Lipiodol group, further indicating that the combination of HmA NPs and DOX could produce better inhibition efficacy for lung metastasis.

3.9. Mechanism of DOX@HmA and Lipiodol combined anti-tumor and anti-metastasis effect

VEGF is a crucial angiogenic factor in tumor tissue that is intimately

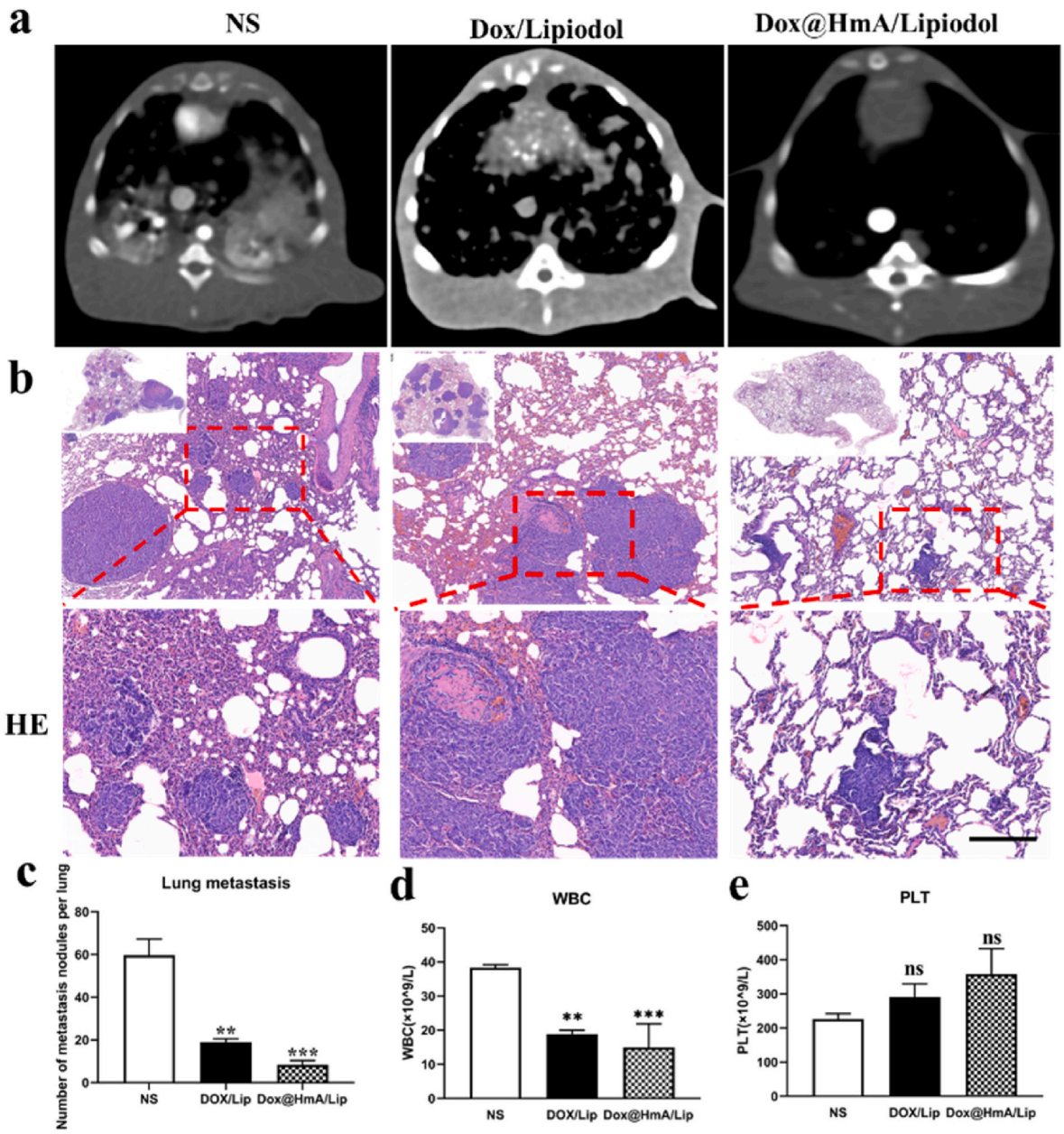

Fig. 8. Representative CT images and HE staining of the lung metastasis in each group 2 weeks after TACE treatment. **(a)** Representative CT images of the lung metastasis for different groups. **(b)** The representative images of HE staining of lung tissues for different groups. HE staining was used to observe the changes in the basic state of the lung. **(c)** The number of metastases per lung in each group was calculated. Data were presented as mean ± SD (n = 3). **(d–e)** The WBC and PLT evaluation of NS, Dox/Lipiodol, Dox@HmA/Lipiodol groups. Scale bar represents 100 μm. (**P < 0.01, ***P < 0.001, ****P < 0.0001).

linked to the processes of tumor angiogenesis and proliferation and is directly implicated in its invasive and metastatic potential. Hence, the expression of VEGF and the residual amount of DOX in tumor tissues were utilized to further investigate and understand the potential mechanisms of DOX@HmA and Lipiodol combined with their anti-tumor and anti-metastasis effects. Representative images of VEGF IF staining of tumor tissues from different groups are shown in Fig. 9a. Compared with the NS group, the fluorescence intensity of the VEGF-positive area in the **DOX@**HmA/Lipiodol and DOX/Lipiodol groups was significantly decreased by IF staining, suggesting a statistically significant difference (Fig. 9b). In addition, the inhibition of VEGF expression in the **DOX@**HmA/Lipiodol group was significantly stronger than that in the DOX/Lipiodol group, suggesting that **DOX@**HmA/Lipiodol interacts with VEGF to inhibit tumor cell proliferation.

Chemotherapeutic drug concentrations in tumor tissues greatly influence anti-tumor activity. Nanodrug delivery systems increase drug accumulating by enhancing the EPR effect of NPs [36]. Meanwhile, in the acidic microenvironment of tumors, the pH-responsive nano-drug delivery system can provide slow and sustained release of drugs, which not only increases the duration of drug action and drug concentration to improve anti-tumor effects but also reduces the systemic drug concentration to decrease the toxic side effects of chemotherapy drugs [37–39]. Therefore, the ability of the HmA system to increase DOX tumor accumulating was evaluated by observing residual DOX in the tumor tissue. As shown in Fig. 9a and c, the fluorescence intensity of DOX in tumor tissues in the **DOX@**HmA/Lipiodol group was also significantly higher than that in the DOX/Lipiodol group, suggesting that **DOX@**HmA NPs could overcome the poor vasculature and dense extracellular matrix in tumors to reach the inside of the tumor mass. Thus, **DOX@**HmA increased the accumulation and drug concentration of DOX in tumor to

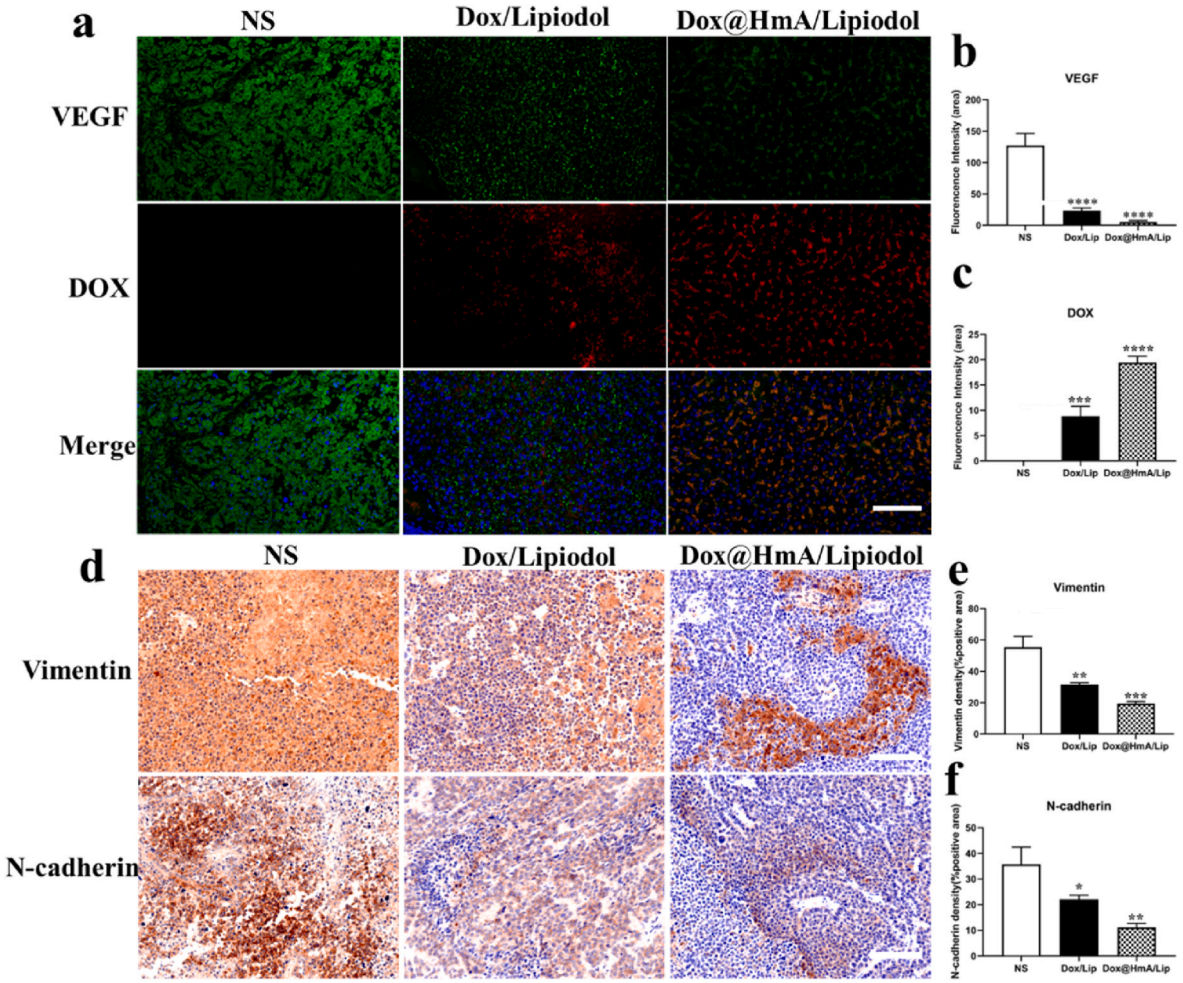

Fig. 9. The mechanism of Dox@HmA and Lipiodol combined anti-tumor and anti-metastasis effect. (a) The representative images of the VEGF immunofluorescence (IF) staining and DOX fluorescence imaging of tumor tissues for different groups, DAPI was used to stain the nucleus. Green fluorescence represents the expression level of VEGF, and red fluorescence represents the content of DOX in tumor tissue. (b) The fluorescence intensity of VEGF positive area in each group was calculated. (c) The fluorescence intensity of DOX-positive area in each group was calculated as the amount of DOX remaining in the tissue. (d) The representative images of the Vimentin and N-cadherin immunohistochemical (IHC) staining of tumor tissues for different groups. (e) The density of Vimentin positive area in each group was calculated in the tissue. (f) The density of N-cadherin positive area in each group was calculated in the tissue. Data were presented as mean ± SD (n = 3). Scale bar represents 100 μm. (*P < 0.05, **P < 0.01, ***P < 0.001, ****P < 0.0001). (For interpretation of the references to color in this figure legend, the reader is referred to the Web version of this article.)

enhance the efficacy of TACE treatment via the polypeptide structure binding to receptors/ligands on the surface of endothelial cells to achieve high selectivity for the tumor microenvironment and active accumulating.

EMT is a key event in tumor cell invasion and metastasis and is a process of tumor cell transformation from epithelial to mesenchymal cells [40]. To further investigate the mechanism by which DOX@HmA/Lipiodol inhibited tumor proliferation and lung metastasis, we performed vimentin and N-cadherin immunohistochemical (IHC) staining of tumor tissues from different groups. As shown in Fig. 9d–f, compared to the NS group, the density of vimentin- and N-cadherin--positive areas in the DOX@HmA/Lipiodol and DOX/Lipiodol groups significantly decreased, especially in the DOX@HmA/Lipiodol group. Thus, **DOX@**HmA inhibited EMT through its anti-tumor and anti-metastasis effects.

4. Conclusion

HmA NPs with DOX enhanced the therapeutic efficacy of TACE for liver VX2 tumors. DOX@HmA NPs showed superior biocompatibility and stability, higher loading capacity, and sustained pH-sensitive release. *In vivo* research proved that the anti-tumor efficacy of the DOX@HmA NPs developed in this study was significantly better than that of DOX, indicating that DOX@HmA NPs increased the accumulation and drug concentration of DOX in tumor, significantly inhibited cell regeneration and tumor angiogenesis, and decreased the systemic side effects of chemotherapy, especially by suppressing pulmonary metastasis in liver VX2 tumors of rabbits by inhibiting EMT. Thus, the DOX@HmA NPs prepared in our study are a promising method for DDSs and provide a new strategy for chemotherapy in clinical TACE and pH-sensitive tumor microenvironment treatments.

Funding

This work was Supported by the National Natural Science Foundation of China (Grant No.81972233), Major scientific and technological innovation project of Wenzhou Science and Technology Bureau (Grant No. ZY2021009, 2021HZSY0069), Natural Science Foundation of Key Laboratory of Diagnosis and Treatment of Severe Hepato-Pancreatic Diseases of Zhejiang Province (No. G2023004, G2023003), Wenzhou high-level innovation team (Development and application team of functional liver cancer-on-a-chip), Zhejiang Provincial Science and

Technology Innovation Program (New Young Talent Program) for College Students (No. 2023R413081).

CRediT authorship contribution statement

Qing Shi: Methodology, Software, Data curation, Writing - original draft. **Xingxing Zhang:** Methodology, Software, Data curation. **Minmin Wu:** Methodology, Software, Data curation. **Yuhan Xia:** Methodology, Investigation. **Yating Pan:** Methodology. **Jialu Weng:** Methodology. **Na Li:** Conceptualization, Supervision. **Xingjie Zan:** Conceptualization, Supervision, Writing - review & editing. **Jinglin Xia:** Conceptualization, Supervision, Writing - review & editing.

Declaration of competing interest

The authors declare that they have no known competing financial interests or personal relationships that could have appeared to influence the work reported in this paper.

Data availability

Data will be made available on request.

References

[1] European Association for the Study of the Liver, Electronic address, easloffice easloffice eu & European association for the study of the, L. EASL clinical practice guidelines: management of hepatocellular carcinoma, J. Hepatol. 69 (2018) 182–236.
[2] M. Omata, et al., Asia-Pacific clinical practice guidelines on the management of hepatocellular carcinoma: a 2017 update, Hepatol Int 11 (2017) 317–370.
[3] J.K. Heimbach, et al., AASLD guidelines for the treatment of hepatocellular carcinoma, Hepatology 67 (2018) 358–380.
[4] A. Forner, M. Reig, J. Bruix, Hepatocellular carcinoma, Lancet 391 (2018) 1301–1314.
[5] J.W. Park, et al., Global patterns of hepatocellular carcinoma management from diagnosis to death: the BRIDGE Study, Liver Int. 35 (2015) 2155–2166.
[6] Y.R. Huo, G.D. Eslick, Transcatheter arterial chemoembolization plus radiotherapy compared with chemoembolization alone for hepatocellular carcinoma: a systematic review and Meta-analysis, JAMA Oncol. 1 (2015) 756–765.
[7] A. Sergio, et al., Transcatheter arterial chemoembolization (TACE) in hepatocellular carcinoma (HCC): the role of angiogenesis and invasiveness, Am. J. Gastroenterol. 103 (2008) 914–921.
[8] W. Ma, et al., The prognostic value of 18F-FDG PET/CT for hepatocellular carcinoma treated with transarterial chemoembolization (TACE), Theranostics 4 (2014) 736–744.
[9] M. Boulin, et al., Improved stability of lipiodol-drug emulsion for transarterial chemoembolisation of hepatocellular carcinoma results in improved pharmacokinetic profile: proof of concept using idarubicin, Eur. Radiol. 26 (2016) 601–609.
[10] D. Kim, et al., Development and evaluation of an ultrasound-triggered microbubble combined transarterial chemoembolization (TACE) formulation on rabbit VX2 liver cancer model, Theranostics 11 (2021) 79–92.
[11] Y. Huang, et al., Trends and Hotspots in nanoparticles for the targeted delivery of nucleic acids: a Ten-Year Bibliometric study, Front. Pharmacol. 13 (2022), 868398.
[12] N. Zhang, G. Xiong, Z. Liu, Toxicity of metal-based nanoparticles: challenges in the nano era, Front. Bioeng. Biotechnol. 10 (2022), 1001572.
[13] L. Gu, et al., Enzyme-triggered deep tumor penetration of a dual-drug nanomedicine enables an enhanced cancer combination therapy, Bioact. Mater. 26 (2023) 102–115.
[14] L. Liu, et al., Periodic mesoporous organosilica-coated magnetite nanoparticles combined with lipiodol for transcatheter arterial chemoembolization to inhibit the progression of liver cancer, J. Colloid Interface Sci. 591 (2021) 211–220.
[15] A. Tasdogan, et al., Metabolic heterogeneity confers differences in melanoma metastatic potential, Nature 577 (2020) 115–120.
[16] A. Brand, et al., LDHA-associated lactic acid production Blunts tumor Immunosurveillance by T and NK cells, Cell Metabol. 24 (2016) 657–671.
[17] H. Li, et al., Recent advances in development of dendritic polymer-based nanomedicines for cancer diagnosis, WIREs Nanomedicine Nanobiotechnology 13 (2021), e1670.
[18] H. Li, et al., Stimuli-activatable nanomedicine meets cancer theranostics, Theranostics 13 (2023) 5386–5417.
[19] L. Js, et al., Sulfamethazine-based pH-sensitive hydrogels with potential application for transcatheter arterial chemoembolization therapy, Acta Biomater. 41 (2016).
[20] S. Li, et al., Smart peptide-based supramolecular photodynamic Metallo-nanodrugs designed by Multicomponent coordination self-assembly, J. Am. Chem. Soc. 140 (2018) 10794–10802.
[21] H. Lopez-Laguna, et al., Assembly of histidine-rich protein materials controlled through divalent cations, Acta Biomater. 83 (2019) 257–264.
[22] S. Wei, S. Zhou, W. Huang, X. Zan, W. Geng, Efficient delivery of antibodies Intracellularly by Co-assembly with hexahistidine-metal assemblies (HmA), Int. J. Nanomed. 16 (2021) 7449–7461.
[23] B. Tang, et al., Decorating hexahistidine-metal assemblies with tyrosine enhances the ability of proteins to pass through corneal biobarriers, Acta Biomater. 153 (2022) 231–242.
[24] W. Huang, et al., Efficient delivery of cytosolic proteins by protein-hexahistidine-metal co-assemblies, Acta Biomater. 129 (2021) 199–208.
[25] H. Xu, et al., Deliver protein across bio-barriers via hexa-histidine metal assemblies for therapy: a case in corneal neovascularization model, Mater. Today Bio 12 (2021), 100143.
[26] W. Huang, et al., Combined delivery of small molecule and protein drugs as synergistic therapeutics for treating corneal neovascularization by a one-pot coassembly strategy, Mater. Today Bio 17 (2022), 100456.
[27] L. Wang, et al., Evaluation of his6-metal assemblies as a drug delivery vehicle in the treatment of anterior segment disease using a corneal Inflammation model, ACS Biomater. Sci. Eng. 6 (2020) 4012–4023.
[28] W. Huang, et al., Hexahistidine-metal assemblies: a promising drug delivery system, Acta Biomater. 90 (2019) 441–452.
[29] P. Bize, et al., Antitumoral effect of sunitinib-eluting Beads in the rabbit VX2 tumor model, Radiology 280 (2016) 425–435.
[30] J.M. Chang, et al., Dynamic contrast-enhanced magnetic resonance imaging evaluation of VX2 carcinoma in a rabbit model: comparison of 1.0-M gadobutrol and 0.5-M gadopentetate dimeglumine, Invest. Radiol. 45 (2010) 655–661.
[31] H. Shao, et al., Diffusion-weighted MR imaging allows monitoring the effect of combretastatin A4 phosphate on rabbit implanted VX2 tumor model: 12-day dynamic results, Eur. J. Radiol. 81 (2012) 578–583.
[32] D.H. Kim, J. Chen, R.A. Omary, A.C. Larson, MRI visible drug eluting magnetic microspheres for transcatheter intra-arterial delivery to liver tumors, Theranostics 5 (2015) 477–488.
[33] T. Minagawa, et al., Activation of extracellular signal-regulated kinase is associated with hepatocellular carcinoma with aggressive phenotypes, Hepatol. Res. 50 (2020) 353–364.
[34] S. Gerstberger, Q. Jiang, K. Ganesh, Metastasis. Cell 186 (2023) 1564–1579.
[35] N.I. Herath, et al., Potentiation of doxorubicin efficacy in hepatocellular carcinoma by the DNA repair inhibitor DT01 in preclinical models, Eur. Radiol. 27 (2017) 4435–4444.
[36] S.K. Golombek, et al., Tumor targeting via EPR: strategies to enhance patient responses, Adv. Drug Deliv. Rev. 130 (2018) 17–38.
[37] W. She, et al., The potential of self-assembled, pH-responsive nanoparticles of mPEGylated peptide dendron-doxorubicin conjugates for cancer therapy, Biomaterials 34 (2013) 1613–1623.
[38] S. Harguindey, S.J. Reshkin, 'The new pH-centric anticancer paradigm in Oncology and Medicine'; SCB, Semin. Cancer Biol. 43 (2017) (2017) 1–4.
[39] E. Spugnini, S. Fais, Proton pump inhibition and cancer therapeutics: a specific tumor targeting or it is a phenomenon secondary to a systemic buffering? Semin. Cancer Biol. 43 (2017) 111–118.
[40] Y. Xu, et al., AFP deletion leads to anti-tumorigenic but pro-metastatic roles in liver cancers with concomitant CTNNB1 mutations, Cancer Lett. 566 (2023), 216240.